Galectin-8 regulates primary cilium in hypothalamic neurons through an L-type calcium channel/Aurora kinase A/HDAC6 pathway impacting body energy balance

Cristian Herrera-Cid[1,3], María Paz Hernández[1,2], Daniela Pinto[1,2], Alejandra Aranguiz[1,2], Francisca Pérez-Molina[1,3], Ariel Vivero[1], Daniela Cortés-Díaz[1,3], Claudia Jara[1,3], Sofia Espinoza[1,3], Andrea Soza[1,3], Cheril Tapia-Rojas[1,3], Bredford Kerr[1], Eugenia Morselli[1,2], Alfonso González[1,3]

[1] Centro de Biología Celular y Biomedicina (CEBICEM) and [2]Departamento de Ciencias Básicas, Facultad de Medicina y Ciencia, Universidad San Sebastián, Santiago, Chile. [3] Centro Científico y Tecnológico de Excelencia (CCTE) Ciencia & Vida.

Corresponding author:

Alfonso González, M.D., Ph.D.

Centro de Biología Celular y Biomedicina

Facultad de Medicina y Ciencia

Universidad San Sebastián

Santiago, Chile.

Address: Lota 2465, Santiago 7510157, Chile.

E-mail: alfonso.gonzalez@uss.cl

Phone number: +56 2 22606300

ABSTRACT

OBJETIVE: Food intake, energy expenditure, and metabolic homeostasis depend on hypothalamic neurons' responses to peripheral signals, such as leptin, involving the primary cilium (PC). The PC is crucial for signal transduction and is dynamically regulated by assembly/disassembly or reabsorption of its microtubules-based axoneme. Absence or reduction in the length of PC is associated with obesity and type-2 diabetes (T2D). In other cellular systems, PC reabsorption is primarily regulated by calcium-mediated activation of the Aurora kinase A (AurkA)/histone deacetylase C6 (HDAC6) axis, which promotes axonemal disassembly. Here, we explore the role of Galectin-8 (Gal-8), a glycan-binding protein, in regulating PC structure and signaling related to metabolic parameters in hypothalamic neurons. METHODS: Gal-8 effects were assessed in hypothalamic Clu-177 cells by analyzing the PC presence and length by immunofluorescence, PC dynamics, and intracellular calcium changes by *in vivo* cell imaging, activation of FAK, Src, AurkA, HDAC6 and STAT3 by immunoblot, and Gal-8 interactions with β1-integrins by pull-down assays. Gal-8-KO mice were used to evaluate PC length in hypothalamic neurons, metabolic phenotype, and responses to Gal-8 intranasal administration. RESULTS: In Clu-177 cells, Gal-8 induced PC reabsorption and reduced responsiveness to leptin signaling towards STAT3 activation. PC reabsorption involves glycan-mediated Gal-8 interactions with a5b1 and a3b1 integrins, activation of FAK and Src leading to calcium influx through L-type calcium channels (LTCC), and subsequent AurkA/HDAC6 axis activation. Gal-8-KO mice showed longer PC in hypothalamic neurons, higher STAT3 activation, decreased body weight and food intake, improved glucose tolerance, higher locomotor activity, and a glycolytic respiratory exchange rate (RER). Daily intranasal Gal-8 administration for 4 days restored hypothalamic PC length and STAT3 signaling, as well as RER in Gal-8-KO mice to the level of WT mice. CONCLUSIONS: Endogenous Gal-8 is required to maintain PC structure and leptin signaling in hypothalamic neurons, impacting body weight, energy balance, and glucose homeostasis. The mechanism involves calcium influx via LTCC downstream of b1-integrin/FAK/Src signaling and subsequent AurkA/HDAC6 axis

activation. Both Gal-8 and the AurkA/HDAC6 axis may offer new therapeutic opportunities for treating metabolic diseases characterized by ciliogenesis impairment, including obesity and type-2 diabetes.

INTRODUCTION

The hypothalamus regulates energy balance by integrating peripheral signals with the central functions of distinct neuronal populations that control appetite and maintain body weight (1, 2). One of the most extensively studied systems is based on discrete groups of neurons concentrated in the arcuate nucleus (ARC) of the hypothalamus and their elaborated circuitries that drive anorexigenic responses to leptin, a hormone secreted by white adipose tissue, particularly after food intake, to induce satiety (3-6). ARC neurons express the long isoform of the leptin receptor, LepRb, which signals through multiple pathways, including tyrosine phosphorylation and activation of STAT3 (7). Alterations in this system due to impaired expression or functional deficiency of leptin or LepRb, as well as various forms of leptin resistance, have long been associated with obesity (7-10). Obesity represents a major public health problem because of its pandemic prevalence worldwide and its predisposition to develop other diseases, such as cardiovascular disorders and type 2 diabetes (11, 12). However, the mechanisms that determine the magnitude of the neural responses to leptin and their dysfunctions that lead to or are associated with obesity have not been fully elucidated (1, 7). It is therefore important to identify endogenous factors in the brain that may affect the sensitivity of hypothalamic ARC neurons to leptin. One aspect that has not been sufficiently explored in this context is the regulation of primary cilium structure, whose features influence the strength of leptin-evoked cellular signaling (13, 14).

The primary cilium (PC) is an antenna-like organelle that protrudes from the surface of most mammalian cells and functions as a sensor of extracellular signals (15). Structurally, it consists of a specialized membrane contiguous with the plasma membrane and a microtubule-based axoneme that extends from the mother centriole of the basal body (15). The PC is highly dynamic, undergoing changes in length or complete loss through tightly regulated processes of assembly, disassembly, and shedding in response to extracellular cues (15-18). This dynamic behavior provides an additional layer of control over intracellular signaling pathways. In neurons, alterations in PC structure have been linked to changes in signaling strength, including pathways mediated by receptors such

as those for leptin and insulin (14, 19, 20). Importantly, defects in PC structure or function underlie a group of disorders known as ciliopathies, which are frequently associated with hyperphagia, early-onset obesity, and type 2 diabetes (13).

Consistent with these observations, the length of the PC in hypothalamic neurons is variable and influenced by dietary conditions and obesity-related states (13, 14, 19), suggesting that endogenous factors regulate the balance between ciliogenesis and PC resorption. Among the signaling pathways affected by PC dynamics, leptin signaling plays a central role in the regulation of energy balance. The hypothalamus integrates peripheral metabolic cues with central neuronal circuits to control appetite and body weight (1, 2). Within this system, neurons located in the arcuate nucleus (ARC) respond to leptin—a hormone secreted by white adipose tissue—by activating anorexigenic pathways that promote satiety (3-5). These neurons express the long isoform of the leptin receptor (LepRb), which signals through multiple pathways, including tyrosine phosphorylation and STAT3 activation (7). Disruptions in leptin production, LepRb function, or downstream signaling are strongly associated with obesity and related metabolic disorders (7-10), a major global health concern due to its increasing prevalence and association with cardiovascular disease and type 2 diabetes (11, 12). Notably, the structural state of the PC has been shown to influence leptin signaling strength in ARC neurons (13, 14). While leptin itself promotes ciliogenesis (14, 20), ciliary dysfunction can lead to leptin resistance even before the onset of obesity (21). However, the endogenous mechanisms that regulate PC maintenance, remodeling, and resorption in these neurons—and how these processes affect leptin responsiveness—remain poorly understood.

Galectin-8 (Gal-8) is a 34 kDa carbohydrate-binding protein broadly expressed across tissues (22-24), including multiple regions of the brain such as the hypothalamus (25-27). Members of the galectin family share conserved carbohydrate-recognition domains (CRDs) with affinity for β-galactosides and are secreted through non-classical pathways (23, 25). Gal-8 contains two distinct CRDs: an N-terminal domain with preferential binding to α2-3-sialylated glycans and a C-terminal domain that recognizes non-sialylated oligosaccharides, connected by a linker peptide that defines different

isoforms (22, 28, 29). Through interactions with cell-surface glycoproteins, Gal-8 regulates diverse cellular processes (22, 23, 25, 30). Among its best-characterized binding partners are β1-integrins, particularly α5β1 and α3β1, whose activation has been shown to increase intracellular calcium levels (23, 27, 31-37). Independently, increases in cytosolic calcium have been linked to PC shortening via activation of calmodulin and Aurora A kinase (AURKA) signaling in both mitotic and non-mitotic cells (38-42). Whether this pathway operates in neurons, however, remains unknown.

In the brain, Gal-8 is expressed in multiple regions, including the hypothalamus (26, 27). In addition to local expression, Gal-8 may also reach the hypothalamus by diffusion from adjacent regions such as the thalamus, as well as from the cerebrospinal fluid (CSF) produced by the choroid plexus, two sites that display the highest levels of Gal-8 expression (26, 27). Components of the CSF can access most regions of the cerebral parenchyma via direct transcytosis across permeable ependymal cells and/or through the glymphatic cerebrospinal fluid–interstitial fluid (CSF–ISF) circulation system (43). Variable levels of Gal-8 have been detected in human cerebrospinal fluid (26). However, to date, the only functions reported for Gal-8 in the brain are neuroprotective and immunosuppressive roles (26, 27). Whether Gal-8 influences hypothalamic neuronal signaling and energy balance regulation has not been explored.

Here, we provide evidence that Gal-8 is a key regulator of primary cilium dynamics and energy balance. Using Gal-8 knockout (Gal-8 KO) mice, we show that endogenous Gal-8 is required to maintain body weight, adipose tissue mass, glucose homeostasis, and the structural integrity of the PC in ARC neurons. Gal-8 deficiency leads to increased PC length and enhanced hypothalamic STAT3 phosphorylation, both of which are reversible upon intranasal Gal-8 administration. Mechanistically, using Clu-177 cells as a model of adult hypothalamic neurons (44), we demonstrate that Gal-8 promotes PC resorption through interaction with β1-integrins, triggering calcium influx and activation of AURKA. This ciliary remodeling is associated with reduced leptin responsiveness. Together, these findings identify Gal-8 as a previously unrecognized regulator of

ciliogenesis in hypothalamic neurons, linking extracellular glycan recognition to the control of energy balance.

RESULTS

Primary cilium length in ARC neurons is increased in Gal-8 KO mice and normalized by intranasal Gal-8 administration

To assess whether Gal-8 influences primary cilium (PC) structure ARC nucleus neurons, we compared PC length in Gal-8 knockout (Gal-8 KO) mice, which lack Gal-8 expression (26, 27), and wild-type (WT) mice. We also evaluated the effect of intranasally administered Gal-8, a non-invasive route for delivering drugs and biologics into the central nervous system with limited peripheral effects (49, 50). Immunostaining of AC3 used as a specific marker for neuronal PC (14, 19) revealed larger PC in the ARC hypothalamic neurons of Gal-8 KO compared to wild-type mice, without significant differences in the percentage of ciliated neurons (Figure 1, A-C). The average PC length increased from 8.36 μm in wild-type mice to 10.64 μm in Gal-8 KO mice (Figure 1, A,B). Analysis of ciliary length distribution showed that WT mice exhibited 17.6% of cilia in the 0–4.9 μm range, 48.8% in the 5–9.9 μm range, and 33.6% exceeding 10 μm, whereas Gal-8 KO mice displayed 5.1% in the 0–4.9 μm range, 41.6% in the 5–9.9 μm range, and 53.3% over 10 μm (Figure 1C). Following intranasal Gal-8 treatment (150ng per day for 4 days), Gal-8 KO mice exhibited an average PC length comparable to that of WT mice, accompanied by a redistribution of cilia lengths to 29.6% in the 0–4.9 μm range, 35.6% in the 5–9.9 μm range, and 34.8% over 10 μm (Figure 1A-C). Thus, intranasal Gal-8 administration partially restored the ciliary length distribution in Gal-8 KO mice, particularly within the 0–4.9 μm and 5–9.9 μm ranges.

Phosphorylation of STAT3 is commonly used as a readout of leptin receptor signaling activity in the hypothalamus (7). Given that PC could be involved in leptin response (13), we next assessed hypothalamic STAT3 phosphorylation levels in Gal-8 KO and WT mice. Gal-8 KO mice exhibited a 1.8-fold increase in hypothalamic STAT3 phosphorylation compared with WT mice (Figure 1D). In contrast, intranasal

administration of Gal-8 to Gal-8 KO mice reduced hypothalamic STAT3 phosphorylation to levels comparable to those observed in WT mice (Figure 1D). Immunohistochemical detection of Gal-8 in the arcuate nucleus further confirmed that intranasally administered Gal-8 reached the hypothalamus (Figure E). Together, these results indicate that endogenous Gal-8 modulates both primary cilium structure and STAT3 signaling in the hypothalamus.

Gal-8 deficiency alters feeding behavior, locomotor activity, and body composition

Given that the leptin–melanocortin circuit regulates appetite and energy expenditure (1, 3, 51), we next compared metabolic and behavioral parameters in wild-type (WT) and Gal-8 knockout (Gal-8 KO) mice. Gal-8 KO mice exhibited lower body weight, reduced food intake, and increased locomotor activity compared with WT mice (Figure 2A–C). We then evaluated the contribution of Gal-8 to fuel selection by measuring the respiratory exchange ratio (RER) in Gal-8 knockout (Gal-8 KO) and wild-type (WT) mice. RER, defined as the ratio of CO_2 production (VCO_2) to O_2 consumption (VO_2), is commonly used to estimate relative carbohydrate versus lipid utilization (52). Gal-8 KO mice exhibited a significantly higher RER (0.95) compared with WT mice (0.87), indicating a shift toward increased carbohydrate utilization (Figure 2D). Consistent with this metabolic profile, intranasal administration of Gal-8 reduced the RER of Gal-8 KO mice to 0.88, closely resembling the WT phenotype (Figure 2D). These results indicate that Gal-8 deficiency alters whole-body substrate utilization, an effect that is reversible upon intranasal Gal-8 administration.

Analysis of body composition in chow-fed animals revealed significant differences between genotypes (Figure 2E-G). Besides the reduction in the body weight, Gal-8 KO mice displayed an increased percentage of total adipose tissue, including total white adipose tissue, inguinal (subcutaneous) white adipose tissue (iWAT), epididymal (visceral) white adipose tissue (eWAT), and interscapular brown adipose tissue (BAT), relative to WT mice. These findings indicate that Gal-8 deficiency affects feeding behavior, physical activity, and adipose tissue distribution.

Since PC function in ARC neurons is implicated in the regulation of insulin signaling and glucose metabolism (1, 3, 51), we next performed glucose tolerance tests (GTTs) in Gal-8 KO and WT mice. Following intraperitoneal glucose administration, Gal-8 KO mice exhibited significantly lower blood glucose levels compared with WT mice. Glycemia was reduced by 32.4% at 30 minutes post-injection and remained lower at later time points, with decreases of 19.5%, 21.7%, and 19.1% at 60, 90, and 120 minutes, respectively (Figure 2H)

These in vivo findings support a role for endogenous Gal-8 in regulating primary cilium structure in hypothalamic neurons, with consequences for metabolic and glucose-related regulation.

Gal-8 induces PC disassembly and resorption in hypothalamic neuron model

To investigate the cellular mechanisms regulating primary cilium (PC) length in hypothalamic neurons, we used CLU-177 cells (also referred to as mHypoA-2/12 cells), an immortalized murine hypothalamic neuronal cell line derived from adult mouse hypothalamus (44). This cell line retains functional leptin receptor signaling and responds to leptin stimulation through activation of canonical JAK2–STAT3 pathways, while expressing feeding-related neuropeptides such as NPY and AgRP (44, 53).

We first assessed the effects of Gal-8 on primary cilium (PC) presence, length, and structure in CLU-177 cells. Based on Gal-8 concentrations reported in human serum, which range from 0.18 to 5 nM in healthy individuals and from 1.34 to 15 nM in patients with proinflammatory conditions or cancer (54, 55), we tested multiple Gal-8 concentrations and identified 30 nM as sufficient to elicit clear effects on PC parameters without inducing cell proliferation (Figure S1). Treatment with Gal-8 (30 nM) for 2 h reduced the percentage of ciliated cells from approximately 80% to 60% (Figure 3A). In the remaining ciliated cells, PC length decreased from an average of 3.64 μm to 2.82 μm, accompanied by a 33.5% reduction in ciliary volume (Figure 3B–D).

To determine the mechanism underlying Gal-8–induced PC loss, we combined live-cell imaging using the SiR-tubulin probe with detection of acetylated α-tubulin in conditioned media, a marker of ciliary shedding (17). Live-cell imaging revealed

progressive PC resorption, detectable within the first 30 min of Gal-8 treatment (Figure 3E). In contrast, immunoblot analysis of conditioned media failed to detect acetylated α-tubulin following 2 h of treatment with 30 nM Gal-8 (Figure 3F). As a positive control for ciliary shedding, treatment with chloral hydrate (CH), a known inducer of PC release (17), resulted in a 2.4-fold increase in the ratio of acetylated α-tubulin to total tubulin in the conditioned media (Figure 3F).

Together, these results indicate that exposure to 30 nM Gal-8 primarily induces PC disassembly and resorption rather than direct ciliary shedding into the extracellular medium.

Gal-8–induced primary cilium loss in hypothalamic neurons model involves activation of β1-integrin–dependent signaling

To determine whether PC loss depends on Gal-8 interactions with cell-surface glycans, we performed competition experiments in which Gal-8 was preincubated with either α-lactose or α2,3-sialyllactose (2,3SL) (28, 32, 56). α-Lactose, which competes with glycan binding to both the N- and C-terminal carbohydrate-recognition domains (CRDs) of Gal-8, completely abrogated Gal-8–induced PC loss. In contrast, 2,3SL, which selectively competes with the N-terminal CRD of Gal-8 (28, 56), partially reduced PC loss from approximately 19% to 9.7% (Figure 4A). Neither sucrose nor α2,6-sialyllactose (2,6SL) affected the ability of Gal-8 to induce PC loss (Figure 4A). Together, these results indicate that Gal-8–induced PC loss requires glycan-dependent interactions with cell-surface components.

Previous studies in multiple cell types have shown that Gal-8 interacts with integrins (23, 25, 30, 32) and induces activation of focal adhesion kinase (FAK), a key signaling component downstream of integrins (26, 31, 32). In addition, Src kinase, another component of integrin-associated focal adhesion complexes, has been reported to inhibit ciliogenesis and reduce primary cilium (PC) size in different cellular contexts (57, 58).

To examine whether these pathways operate in hypothalamic neurons, we performed pull-down assays and found that Gal-8 interacts with integrin α3 and integrin α5 in CLU-177 cells (Figure 4B). Immunoblot analysis further revealed that Gal-8 rapidly

activated both Src and FAK, with increases of 21% and 28%, respectively, detectable within 5 min of stimulation (Figure 4C). Preincubation of cells with the Src inhibitor PP2 (20 μM) or the FAK inhibitor Y15 (10 μM) prior to Gal-8 exposure prevented Gal-8–induced PC loss (Figure 4D).

Together, these results indicate that Gal-8–mediated PC resorption in CLU-177 cells involves integrin engagement and activation of downstream FAK and Src signaling.

Gal-8–induced β1-integrin/FAK/Src signaling promotes LTCC-mediated calcium influx, AURKA/HDAC6 activation, and primary cilium loss

Gradual PC resorption has been shown to depend on calmodulin-mediated activation of Aurora A kinase (AURKA) downstream of elevations in cytosolic calcium (38-40). Activated AURKA, in turn, phosphorylates and activates histone deacetylase 6 (HDAC6) (16, 41), which deacetylates and destabilizes α-tubulin, promoting axonemal depolymerization and PC resorption (38, 40). We therefore examined whether this pathway operates in our cell model following Gal-8 stimulation.

Ratiometric calcium imaging revealed that Gal-8 treatment induced a rapid increase in cytosolic calcium concentration, peaking within 10–15 s (Figure 5A). Chelation of extracellular calcium by addition of EGTA to the culture medium completely abolished this calcium rise and concomitantly prevented Gal-8–induced PC loss (Figure 5A-B). These results indicate that Gal-8–induced PC resorption requires calcium influx.

Activation of α5β1 integrin has been reported to induce calcium influx through opening of L-type calcium channels (LTCCs) in a Src- and FAK-dependent manner (34, 35). We detected expression of the LTCC isoform CaV1.3 in CLU-177 cells (Figure 5C). Pretreatment with the LTCC blocker nifedipine (20 μM) completely abrogated the Gal-8–induced increase in cytosolic calcium levels (Figure 5D). Inhibition of FAK and Src using Y15 (10 μM) and PP2 (20 μM), respectively, similarly prevented Gal-8–induced cytosolic calcium elevations (Figure 5E).

Consistent with activation of the calcium-dependent ciliary resorption pathway, Gal-8 treatment increased HDAC6 phosphorylation by approximately 45% (Figure 6A). Pretreatment with the AURKA inhibitor VX-680 prevented both HDAC6 phosphorylation

and Gal-8–induced primary cilium loss (Figure 6A-B). Notably, blockade of calcium entry with nifedipine also inhibited Gal-8–induced HDAC6 activation (Figure 5C).

Together, these results indicate that Gal-8 induces LTCC opening downstream of β1-integrin–mediated FAK and Src activation, and that the resulting calcium influx promotes primary cilium resorption through activation of the AURKA–HDAC6 axis.

Gal-8 attenuates leptin-induced STAT3 phosphorylation in CLU-177 cells.

Alterations in primary cilium biogenesis and structural integrity in hypothalamic neurons have been shown to impair leptin signaling pathways (13, 14, 19, 20). Leptin signaling was therefore assessed by immunoblot analysis of STAT3 phosphorylation at Tyr705, a downstream event dependent on LepRb activation (59). Stimulation of CLU-177 cells with leptin (100 nM) induced an approximately 73% increase in STAT3 phosphorylation. In contrast, pretreatment with Gal-8 markedly reduced leptin-induced STAT3 phosphorylation to approximately 17% (Figure 6D).

These results indicate that Gal-8 treatment diminishes leptin/LepRb signaling in hypothalamic cells, in association with Gal-8–induced primary cilium resorption.

Discussion.

This study provides evidence of Gal-8 as a novel regulator of metabolic homeostasis. The characterization of Gal-8-KO mice phenotype together with studies in the hypothalamic cell line CLU-177/mHypoA-2/12 indicate that Gal8 is required to maintain adequate fuel use and adipose tissue content by modulating the structure and signaling properties of PC in hypothalamic neurons. Gal-8 KO mice exhibited longer PCs and increased STAT3 phosphorylation, reflecting an enhanced leptin signaling in the hypothalamus, together with alterations in hypothalamic-regulated metabolic parameters, which can be normalized by intranasal Gal-8 administration. A mechanistic approach in the CLU-177/mHypoA-2/12 cells shows that Gal-8 induces PC disassembly and resorption via LTCC-mediated calcium influx and a subsequent activation of the AurkA/HDAC6 axis, downstream of the β1-Integrin/FAK/Src signaling pathway. Gal-8 and

AURKA/HDAC6 pathways may offer new therapeutic opportunities for metabolic disorders derived from hypothalamic PC dysfunctions.

We found that Gal-8-KO mice are leaner, eat less, and have higher locomotor activity than WT mice, but display increased accumulation of both white and brown adipose tissue. This suggests that the absence of Gal-8 alters energy utilization rather than caloric intake. In line with this possibility, Gal-8-KO mice have elevated RER, indicating of a shift towards the less efficient glycolytic metabolism compared with oxidative metabolism. This metabolic shift may contribute to an adipose tissue accumulation secondary to impaired fatty acid oxidation.

These findings correlate with an exacerbated PC length and function, which would promote leptin signaling towards appetite reduction and increased energy expenditure, contrasting with shortened PCs (13, 14, 20). In Gal-8-KO mice, close to 58% of the neurons in the arcuate nucleus of the hypothalamus, probably including both POMC and AgRP neurons, show longer PCs with length in the range of 10-20 μm. PCs in neurons of the arcuate nucleus contribute to insulin signaling and, thus, regulation of glucose metabolism (3, 19, 51). We found improved glucose tolerance in the GTT of Gal-8 KO mice. This property, together with the preferential glycolytic RER may be attributed to higher sensibility to leptin and insulin stimuli in hypothalamic neurons. These results suggest a role for endogenous Gal-8 in the maintenance of appropriate PC length in hypothalamic neurons, possibly by counteracting endogenous stimuli of ciliogenesis, such as leptin and insulin (14, 20).

Interestingly, blood miRNAs that control Gal-8 expression have been found to be reduced in obesity, predicting higher Gal-8 expression levels, yet in unknown tissues (60-62). PC alterations in neurons that express leptin receptor in other brain regions (3, 51, 63), or PC-dependent insulin and MC4R signaling (3, 19, 51, 64), as well as possible unknown functions of Gal-8 in peripheral tissues (23, 30), may contribute to the metabolic phenotype of Gal-8 KO mice.

Intranasal administration is a non-invasive route to deliver drugs or biologically active components into the CNS with limited peripheral spread (49, 65). This route has

been widely characterized for insulin effects on cognitive dysfunctions of Alzheimer's patients (49) and food intake in healthy individuals (66). In rats with metabolic syndrome, nasal insulin normalizes glycemia and reduces weight (67). Proteins can rapidly reach the hypothalamus after nasal administration, as shown for radiolabeled-albumin, which becomes detectable 5 minutes after administration and reaches its peak concentrations in 1 hour (50). We evaluated the effect of intranasal administration of Gal-8 in KO mice and found it to restore PC structure, STAT3-related activity, and RER close to the values observed in WT mice. These results reinforce the possibility that Gal-8 acts as a new regulator of PC-dependent metabolic balance in the brain.

The longer PC found in Gal-8-KO mice suggests that Gal-8 might negatively regulate cilia length. Our experiments in CLU177 cells show that just within 2 hours of treatment, Gal-8 reduces by ~60% the number of cells bearing PC and decreases by ~22.5% the length of their remaining PC. The evidence suggest resorption instead of shedding as the main mechanism of Gal-8-induced PC loss, as we found progressive PC shortening and undetectable acetylated α-tubulin as a PC component in the medium. This contrasts with the shedding process described as the prevalent PC-loss mechanism induced by serum (17). The difference very likely reflects distinct intracellular pathways affecting PC architecture. Serum stimulation likely involves PDGF and other components (38), including lysophosphatidic acid and PI3K/AKT activation (68), whereas Gal-8 mainly activates β1-integrin-mediated signaling towards FAK and Src (26, 27, 31, 32).

We show that β-lactose, currently used to block galectin interactions with glycans (26, 27, 31, 32), abrogates Gal-8-induced PC loss, thus demonstrating its dependency on Gal-8 interactions with cell surface glycans. Gal-8's N-terminal carbohydrate recognition domain (CRD) prefers terminal α-2,3-sialyllactose, whereas its C-terminal CRD shares with other galectins the general preference for N-acetylactosamines (28, 56). We also show that α-2,3 but not α-2,6 sialyllactose prevents Gal-8-induced PC loss, indicating a selective requirement of glycan interactions with Gal-8's N-terminal CRD.

Integrins are the main counter-receptors of Gal-8 (23, 25, 30), and their activation, followed by downstream FAK/Src kinase signaling, regulates diverse cellular processes

(23, 25, 27, 30-32). In line with previously described interactions of Gal-8 with cell surface glycoproteins in other cellular systems (26, 27, 31, 32), including hippocampal neurons (27), our pull-down experiments show that Gal-8 preferentially binds α3- and α5- but not α4- β1-integrins in CLU177 cells. Accordingly, we found that Gal-8 treatment activates FAK and Src and also that their inhibitors prevent the PC loss. These results implicate the β1integrin/FAK/Src pathway in the PC resorption process.

Previous studies describe that activation of α5β1 integrins with ligands such as RGD peptides, fibronectin, or anti-a5 antibodies induces calcium influx via LTCC downstream of FAK and Src in basal forebrain neurons and vascular smooth muscle cells, two types of excitable cells (34, 35). This effect involves an α5β1 interaction with LTCC (33). Also, overexpression of α3β1-integrin, as found in tumor-associated endothelial cells in glioblastoma, promotes calcium influx, though the mechanism has not yet been elucidated (37). Gal-8 itself induces calcium influx in platelets via an unknown mechanism (69). Here, we show that Gal-8 triggers calcium increments in CLU177 cells, mitigated by EGTA, implying calcium influx. This calcium influx is abrogated by the LTCC inhibitor Nifedipine, as well as by FAK or Src inhibitors, indicating that Gal-8 triggers the described α5β1/FAK/Src/LTCC pathway resulting in calcium influx in CLU177 (34, 35). As expected, this calcium influx activates AURKA and HDAC6, and their inhibition, as well as all conditions that prevent calcium influx, impedes PC loss induced by Gal-8 in CLU177 cells. AURKA is known to phosphorylate the deacetylase HDAC6, enhancing its deacetylase activity, which deacetylates the polymerized α-tubulin of the PC axoneme and promotes its disassembly without affecting non-ciliary acetylated microtubules in the cytoplasm (38). HDAC6 also deacetylates cortactin, which leads to actin polymerization, additionally contributing to PC disassembly (70). Altogether, these data indicate that Gal-8, acting through a selective β1-integrin/SRC/FAK/LTCC pathway, triggers a well-known mechanism of PC resorption involving AURKA/HDAC6 activation by cytosolic calcium increase. Our results are the first to demonstrate that Gal-8 activates this mechanism of PC regulation.

Leptin controls feeding, maintains energy homeostasis, and regulates glucose metabolism by activating its receptor LepRB, which is highly expressed by antagonistic POMC and AgRP neurons in the arcuate nucleus of the hypothalamus, as well as by neurons of other brain regions involved in neuroendocrine control (51, 63). Leptin-activated LepRB triggers downstream signaling pathways that include JAK2-STAT3 (71). Previous work identified LepRB at the base of the PC and suggests that functional PCs are necessary for appropriate leptin signaling in the hypothalamus (13, 14). Our results show that Gal-8 pretreatment decreases leptin signaling towards STAT3. Therefore, Gal-8 can potentially regulate PC-dependent leptin functions affecting food intake and energy balance (13).

Previous studies using Gal-8-KO mice and experimental autoimmune encephalomyelitis, a model of multiple sclerosis, suggested a role of Gal-8 as immunosuppressor protecting against damaging neuro-inflammatory conditions in the brain (26). A neuroprotective role of Gal-8 has also been proposed from experiments in neuronal primary cultures and stereotaxic injection of a damaging agent such as H_2O_2 in hippocampus (27). We have described the presence of circulating anti-Gal-8 autoantibodies in systemic lupus erythematosus (SLE), rheumatoid arthritis, during sepsis (72) and in multiple sclerosis (MS) (26), which can be function-blocking (26, 31, 73, 74), and able to neutralize the immunosuppressive and neuroprotective roles of Gal-8 (26, 27). Their potential pathogenic roles have so far been associated with lymphopenia in SLE (72) and with worse prognosis in patients with the relapsing-remitting form of MS (26). It is also possible that circulating anti-Gal-8 autoantibodies reach the hypothalamus by diffusing from the fenestrated capillaries of the nearby medial eminence (75) and block the function of Gal-8 on the neuronal PC, leading to metabolic alterations.

Glycan structural changes that affect the interactions of galectins with cells can occur in physiological or pathological conditions (76, 77). The so-called “glycan code” is dynamically translated by lectins, including galectins, in different organs and systems (25, 76-78), associated with metabolic alterations, including obesity and alteration in glucose homeostasis (76). N-acetylglucosamine (GlcNAc), which promotes N-glycan branching

and affinity changes for galectins (76, 79), have been found to correlate with insulin resistance and weight gain in mice when dietary supplement or derived from the gut microbiota (79, 80). On the other hand, secreted neuraminidases release sialic acid from cell surface glycans and thus decrease their interactions with Gal-8 (81-84). Peripheral organs such as the liver show increased sialylated glycans in obesity (85, 86). Mice receiving a high-fat diet display reduced expression of neuraminidase Neu1 associated with insulin resistance and hyperglycemia (87). Interplays between N-Glycan branching and sialylating/desialylating conditions affecting Gal-8-dependent PC functions in the hypothalamus, need to be investigated in the future.

Non-mitotic AURKA roles have been increasingly explored since its first identified involvement in PC disassembly during G/G1 cell cycle phase (41). However, the only function of AURKA described in post-mitotic neurons is related to neurite extension, which involves PKC–AURKA–NDEL1 signaling axis (41, 88). The crucial role of the PC in transducing metabolic signals from leptin, insulin and MC4R (13, 14, 19, 64), suggests that AURKA, together with its variety of protein interactors, regulators, and effectors (16, 41, 89), may be important players in the regulation of the neuroendocrine system, with potential therapeutic applications. Genetic human disorders and preclinical models of some ciliopathies may be directly connected to the regulation of AURKA (40-42). For instance, INPP5E, a protein defective in MOMR ciliopathic syndrome that includes obesity, seems to form a positive feedback loop of mutual activation with AURKA, suppressing ciliogenesis (41, 42). Ciliogenic promoting actions of leptin and insulin (14, 20), as well as the recently described shortening and loss of the PC in hypothalamic neurons exposed to palmitic acid or high-fat diets leading to insulin resistance (19), may involve known regulators of the AURKA/HDAC6 axis.

New translational opportunities may arise from our results. For instance, specific AURKA inhibitors used in clinical tests against cancer (41), and L-type calcium channel inhibitors, such as Nifedipine used in hypertension (90), might be repurposed to promote hypothalamic ciliogenesis associated with the control of appetite and metabolic homeostasis. A similar approach may stimulate searching for specific Gal-8 inhibitors (91).

Exploration of intertwined AURKA and Gal-8 pathways could lead to innovative therapies for metabolic disorders, emphasizing the significance of these proteins in maintaining metabolic homeostasis and offering new avenues for clinical intervention.

Methods

Animals

Male mice, 3-4 months old, were housed at the Faculty of Biological Sciences of the Pontificia Universidad Católica de Chile, and maintained under conditions of strict confinement, including automatic control of temperature (21°C) and photoperiod (12 h light / 12 h dark), with water and food ad libitum. All protocols were approved by the Institutional Ethics Committee of Care and Use of Animals in Research of Universidad San Sebastián (protocol number 21-2021-20). Lgals8/Lac-Z knock-in (here Gal-8-KO) mice have Lgals8 gene (18,427 bp) replaced with LacZ lox-Ub1-EM7-Neo-lox Cassette containing the LacZ gene that encodes b-galactosidase (26, 27). Animals were randomly assigned to control or test groups for each experiment and maintained in the same environment to avoid bias. Each animal was considered an individual experimental unit. Body weight was measured using a mouse scale (Accuris Instruments, Model W3300-500). food intake and locomotor activity were measured for 12 h in the dark cycle using a Metabolic Cage (Ugo Basile S.R.L. Model 41800-010).

Regents and materials

The following reagents were purchased from Sigma: Thrombin from human plasma (T1063), bacterial protease inhibitor cocktail (P8465), Src inhibitor PP2 (P0042), FAK inhibitor Y15 (SML0837), and protease and phosphatase inhibitor tablets (A32959, Pierce). Reagents from Santa Cruz Biotech included: Nifedipine (SC-3589), and antibodies against α-tubulin (B-5-1-2), Cav a1D (E3), a-3 (A-3), a-5 (H-104) and b1 (4B7R) integrins, FAK (H-1), pFAK (2D11), Src (B-12) and pSrc (9A6). Cell Signaling Technology provided antibodies against acetylated-α-tubulin K40 (D2063), HDAC6 (D21B10), STAT3 (D3Z26) and pSTAT3 (M9C6). Anti-pHDAC6 (Ab61058) was purchased in Abcam. Secondary antibodies conjugated with horseradish peroxidase or AlexaFluor were

obtained from Rockland and Molecular probes, respectively. Glutathione-sepharose 4B (17075601) (Cytiva), isopropyl-1-thiogalactopyranoside (IPTG) (Invitrogen) SiR-Tubulin (CY-SC002;Cytoskeleton), Fura-Red AM (Cat # F3020;Invitrogen)

Cell culture.

Clu-177 cells were maintained with high glucose Dulbecco's Modified Eagle's medium (DMEM) supplemented with 10% Fetal Bovine Serum, 100 ug/mL penicillin, and 0,1 mg/mL of streptomycin (P/S) in a cell incubator with a constant flow of 95% O2 and 5% CO2 at 37 °C. Cells were tested for mycoplasma contamination every two weeks. Eighteen hours prior to the experiments, cells at 70% confluency were washed with PBS 1x and maintained with DMEM-P/S media without FBS to induce ciliogenesis (17).

Recombinant Gal-8 production

Human recombinant Galectin-8 (Gal-8) was produced as previously described (27). Briefly, bacteria transformed with pGEX-4T-3 (Pharmacia Biotech) plasmid bearing Gal-8-GST or GST were grown in a pre-inoculum in LB supplemented with ampicillin (100 µg/ml) (LB/Amp) at 37°C and 200 RPM of agitation. Gal-8-GST production was induced by IPTG (0.1 mM). Bacterial pellets were lysed for total protein extraction, and Gal-8-GST was purified via a Glutathione-Sepharose column. Gal-8 was released from GST-Gal-8 linked to glutathione-Sepharose by thrombin treatment (10 U/mg of fusion protein) for 4 h at room temperature.

Immunofluorescence.

Clu-177 cells were fixed with ice-cold paraformaldehyde (PFA) and 4% sucrose for 10 min and incubated with blocking buffer (TBS/Saponin 0.05%/BSA 1%) for 30 minutes at RT. Cells were then incubated overnight with primary antibody diluted in blocking buffer at 4°C, followed by secondary antibody conjugated with AlexaFluor and Hoechst for 1 h at 37ºC and finally mounted with Fluoromount. Arcuate nucleus slices, prepared as previously described (19), were incubated overnight at 4°C with the primary antibody against adenylate cyclase 3 (AC3) or Gal-8. Slices were then incubated with secondary antibodies for 1 h at room temperature and mounted with Fluoromount. Slides stained with NeuroTrace probe were dyed according to the manufacturer's instructions.

Analysis of PC morphology

The percentage of cells with primary cilia (PC) was evaluated by counting the number of ciliated cells versus their total number in at least 100–150 cells per sample from three different experiments. PC images were captured by z-stacking on a Leica SP8 or Zeiss AiryScan confocal microscope. PC morphology was analyzed using the FIJI plugin CiliaQ, as described by Hansen et al (45).

Western Blots

Cells exposed to the different treatments were lysed with RIPA lysis buffer (Tris 50 mM, NaCl 150 mM, EDTA 5 mM, NP40 1%, Sodium Deoxycholate 0.5%, SDS 0.1%, pH 8.0) for 30 minutes at 4°C, supplemented with protease and phosphatase inhibitors. Samples were resolved in an SDS-PAGE gel and transferred onto a PVDF membrane using the Bio-Rad Trans-Blot Turbo system. Membranes were blocked, and primary antibodies were incubated overnight at 4ºC in blocking buffer. Secondary antibodies were incubated for 1 h in blocking buffer at 37ºC. Images were acquired using the Syngene G:Box detection system, and densitometric band analysis was performed using FIJI software.

Pull-down assay

Protein extracts were preincubated with GST-Glutation Sepharose column for 1 h at 4ºC, then incubated for 2 h at 4ºC with Gal-8-GST-Glutation-Sepharose. The bound protein was eluted and analyzed by immunoblot, as previously described (26).

Conditioned media analysis.

Clu-177 cells were treated with Gal-8, vehicle or Shedding Cilia Buffer (46) (SCB) (112 mM NaCl, 3.4 mM KCl, 10 mM CaCl2, 2.4 mM $NaHCO_3$, 2 mM HEPES, pH 7.0). The conditioned media was centrifuged at 1,000g x g for 10 min to remove cell debris, and the supernatant was incubated with 20% trichloroacetic acid (TCA) overnight at 4°C with agitation. Samples were centrifuged at maximum speed for 10 min and prepared for western-blot analysis.

PC live cell imaging.

Clu-177 cells seeded in live cell imaging plates were incubated with 100 nM SiR-Tubulin overnight, washed twice with 1mL of DMEM-Hepes, and live cell imaging was performed with a Leica SP8 confocal microscope, using a 63x oil immersion objective and time resolution of 180 seconds per frame.

Ratiometric calcium imaging.

Clu-177 cells were incubated with 5 uM Fura-red AM for 30 minutes. Pre-treatments with blockers or inhibitors were performed post incubation with Fura-red AM. Live cell imaging was performed with a Leica SP8 confocal microscope with a 63x oil immersion objective and a time resolution of 5 seconds per frame.

Locomotor activity.

Mice were placed in a metabolic cage (UGO BASILE, model 41801) for seven hours, and then their locomotor activity was measured during the night phase for 12 hours, with food and water *ad libidum.*

Respiratory exchange ratio.

CO_2 production and O_2 consumption were measured using the iWorx GA200 measurement system according to the manufacturer's instructions. Mice were placed in the metabolic cage at a maximum concentration of 0.24% CO_2. Measurements were performed until a CO_2 concentration of 3% was achieved. Data were analyzed with the LabScribe 2.0 software according to the manufacturer's instructions.

Glucose tolerance test.

The mice's basal glycemia was measured after 6 hours of fasting. A glucose solution (2 g per kg of body weight) was injected subcutaneously. Glycemia measurements were performed every 30 minutes post-injection for 2 hours. During the measurement period, the mice were deprived of food to avoid interference with the measurement (47).

Body fat composition.

To evaluate body fat composition of WT and Gal-8-KO mice, after euthanasia, interscapular brown adipose tissue (BAT), inguinal (subcutaneous) white adipose tissue

(iWAT) and epidydimal (visceral) white adipose tissue (eWAT) was extracted and weighed.

Intranasal Gal-8 administration.

Intranasal administration of Gal-8 was performed in 3-month-old Gal-8-KO mice partially anesthetized with isoflurane as previously described (48). In brief, in a prone position, 3 uL of Galectin-8 (50 mg/ml) or PBS was administered to the treated or control group, respectively, in each nostril. The procedure was repeated once a day for 4 days.

Statistical analysis.

Analyses were conducted with GraphPad Prism 8.0 software. Student’s t-test was used for two-group comparison, and one-way or two-way analysis of variance (ANOVA) with Tukey's multiple comparisons test was used for comparisons of more than two groups. P-values equal to or minor than 0.05 ($P \leq .05$) were considered statistically significant. The confidence interval range was 95% in all tests. The p-value graphic style is indicated according to APA format.

ACKNOWLEDGMENTS

Funding: FONDECYT grants #1221796 (A.G.), #1240623 (E.M), #1211829 (A.S.) #1221178 (C.T.), #1230905 (B.K.), and Anillo ACT #210039 (B.K.); FONDECYT Postdoctorado #3210630 (M.H.), ANID Centro Científico Tecnológico de Excelencia Ciencia & Vida Basal Project FB210008 (AG, AS, CT). ANID BECAS DOCTORADO NACIONAL 21211974 (C.H.). USS VRID_INTER22/18 (C.H.).

AUTHOR'S CONTRIBUTION: C.H.: Conceptualization, Data curation, Formal analysis, Validation, Visualization, Investigation, Methodology, Writing**. M.H; D.P.; A.A.; F.P.; A.V.; D.C. C.J., S.E.:** Investigation, Methodology**,** Data curation. **E.M, B.K and C.T.:** Conceptualization**,** Resources, Data curation, Writing**. A.S.:** Resources, Conceptualization, Writing. **A.G.:** Founding Acquisition, Resources, Conceptualization, Data curation, Supervision, Validation, Writing.

DISCLOSURE STATEMENT: The authors declare that no conflicts of interest exist.

Figure 1. PC length, STAT3 signaling and Respiratory Exchange Ratio (RER)in Gal-8 KO mice after intranasal Gal-8 treatment

WT, Gal-8-KOmice and Gal-8-KO mice non- and treated with daily intranasal administration of PBS alone (vehicle) or Gal-8 (50 ug/ml in PBS) were analyzed for: A) Confocal images of neuronal adenylate cyclase 3 (green) immunoreactivity in the hypothalamus arcuate nucleus; B) PC length; C) PC length distribution(WT and Gal-8-KO n=7; Gal-8-KO+PBS and Gal-8-KO+Gal8,n=5; ***P<0.001; One-way Anova, SD); D) Immunoblot of STAT3 phosphorylation(***P<0.001; One-way Anova, SEM); and E) Immunohistochemistry against Gal-8 (red) and neuron staining with NeuroTrace (green) of arcuate nucleus cryosections, showing that intranasally added Gal-8 reaches the hypothalamus(n=5).

Figure 2. Gal-8-KO mice have metabolic alterations.

Gal-8 KO mice show lower weight (A) and food intake (B), as well as an increased locomotor activity (C) compared with WT mice (n=7; P<0.01**, P<0.05*; t-test, SEM) and D) Respiratory exchange ratio (RER) of WT and Gal-8-KO mice (n=7, ***P<0.001; One-way Anova, SEM).E)Body fat composition of WT and Gal-8-KO mice. Total adipose tissue (AT) percentage and White adipose tissue (WAT). F-G) Inguinal white adipose tissue (iWAT) percentage, Epididymal white adipose (eWAT) percentage and Interscapular brown adipose tissue (BAT). WT n=10; KO n=3 biologically independent animals. H) Glucose tolerance test shows lower pick at 30 min and faster decrease of glucose levels in Gal-8 KO compared with WT mice (n=7, ***P<0.001, *P<0.05; Two-way Anova, SEM).Data are presented as mean ± SEM values and differences were analyzed with unpaired t-test, statistical significances correspond to ***P≤0.001, ****P≤0.0001.

Figure 3. Galectin-8 induces resorption of PC in CLU-177cells.

A) Indirect immunofluorescence against acetylated α-tubulin (red) showing the PC in Clu-177cells treated with 30nM of Gal-8 or denatured Gal-8 (dnGal-8) for 2 hours. Gal-8, but not dnGal-8, reduced the number of ciliated cells from 79.9% to 59.8% (P<0.001; One-

way Anova, SEM); B-D) Gal-8, but not dnGal-8, treatment decreased PC length (B and C) and ciliary body volume (D). E) Live cell imaging of Clu-177cells stained with SiR-Tubulin shows PC resorption in cells treated with 30 nM Gal-8 compared with untreated cells; F) Cells stained against acetylated α-tubulin after incubation in conditioned media of cells treated with 30 nM Gal-8 or Cilia Shedding Buffer (CSB)at the indicated time points. (P<0.001; One-way Anova, SEM).

Figure 4. Gal-8-induced loss of PC involves interactions with cell surface glycans and b1-integrins followed by FAK/Src activation.

A) Percentage of ciliated Clu-177cells treated with Gal-8 (30 nM) in the absence or presence of 10 mM α-2,3-syalillactose (2,3SL), α-2,6-syalllactose (2,6SL), or lactose. Only 2,3SL and lactose prevented Gal-8-induced PC loss. (**P<0.01 or ***P<0.001; One-way anova, SEM). B) Gal-8-GST pulldown assay shows a Gal-8 interaction with α3, α5 and β1 integrin subunit; C and D) Gal-8 (30nM, 5 min.) treatment for increased Src and FAK phosphorylation in Clu-177cells. (P<0.05; t-test, SEM). E) Src and FAK inhibitors, PP2 and FAKi, respectively, prevented PC loss induced by Gal-8 (30nM, 2h) treatment (P<0.001, One-way Anova, SEM).

Figure 5. Gal-8 induces PC resorption through LTCC-associated calcium influx.

A) Cytosolic calcium levels measured by Fura-Red AM imaging. Gal-8 treatment induced an increase in intracellular calcium levels, which are abrogated by EGTA, thus indicating a calcium influx; B) The PC loss elicited by Gal-8 is avoided by co-treatment with EGTA, indicating its dependency on the induced calcium influx (***P<0.001; One-way ANOVA, SEM);C) LTCC (L-type calcium channel Cav 1.3)expression. The immunoblot shows the LTCC regulatory subunit α1Din extracts of Clu-177 cells; D) Pretreatment with L-type calcium channel blocker Nifedipine (NIFE), as well as Src and FAK inhibitors (PP2 and FAKi, respectively), abrogates the calcium influx induced by Gal-8 treatment.

Figure 6. Gal-8-induced PC loss depends on calcium-mediated activation of the AurkA/HDAC6 axis.

A) Immunoblot of AURKA-dependent HDAC6 phosphorylation at S22. Cells treated with Gal-8 for 2 h show an increased phosphorylation of HDAC6 at S22, which is impeded by the AurkA inhibitor VX-680, indicating that Gal-8inducesHDAC6 activation downstream AurkA activity (**P<0.01; One-way anova, SEM); B) Immunofluorescent analysis of PC presence in Clu-177 cells. The PC loss induced byGal-8 (30nM) treatment for 2 hours decreases under pretreatment with AurkA inhibitor VX-680 (P<0.01; One-way Anova, SEM); C) Calcium channel inhibitor, Nifedipine, abrogates the HDAC6 activation induced by Gal-8 (**P<0.01; One-way Anova, SEM).D) Immunoblot against phosphorylated STAT3 (pSTAT3), as a measurement of Leptin-induced signaling. Pre-treatment with Gal-8 for 2 h, which leads to PC loss as in A), decreases STAT3 activation in response to Leptin (100 nM) stimulation for 1hour. Graph shows quantification of the effect (**P<0.01, ***P<0.001; One-way Anova, SEM).

References

1. Friedman JM. Leptin and the endocrine control of energy balance. Nat Metab. 2019;1(8):754-64.

2. Schwartz MW, Woods SC, Porte D, Jr., Seeley RJ, Baskin DG. Central nervous system control of food intake. Nature. 2000;404(6778):661-71.

3. Lavoie O, Michael NJ, Caron A. A critical update on the leptin-melanocortin system. J Neurochem. 2023;165(4):467-86.

4. Solheim MH, Stroganov S, Chen W, Subagia PS, Bauder CA, Wnuk-Lipinski D, et al. Hypothalamic PNOC/NPY neurons constitute mediators of leptin-controlled energy homeostasis. Cell. 2025;188(13):3550-66 e22.

5. Gou Y, Glat M, Damian V, Bryan CL, Phan BA, Faber CL, et al. AgRP neuron hyperactivity drives hyperglycemia in a mouse model of type 2 diabetes. J Clin Invest. 2025;135(10).

6. Lavoie O, Michael NJ, Caron A. New players in the leptin orchestra: PNOC/NPY neurons tune appetite and obesity. Neuron. 2025;113(12):1855-7.

7. Liu H, Du T, Li C, Yang G. STAT3 phosphorylation in central leptin resistance. Nutr Metab (Lond). 2021;18(1):39.

8. Caron A, Lee S, Elmquist JK, Gautron L. Leptin and brain-adipose crosstalks. Nat Rev Neurosci. 2018;19(3):153-65.

9. He W, Loganathan N, Tran A, Belsham DD. Npy transcription is regulated by noncanonical STAT3 signaling in hypothalamic neurons: Implication with lipotoxicity and obesity. Mol Cell Endocrinol. 2024;586:112179.

10. Oclon E, Gurgul A, Szmatola T, Jasielczuk I, Kucharski M, Zubel-Lojek J, Zieba DA. Impact of modulating leptin sensitivity on the transcriptomic profile of adult-derived hypothalamic mouse neurons. Front Mol Neurosci. 2024;17:1518737.

11. Le Thuc O, Garcia-Caceres C. Obesity-induced inflammation: connecting the periphery to the brain. Nat Metab. 2024;6(7):1237-52.

12. Boutari C, Mantzoros CS. A 2022 update on the epidemiology of obesity and a call to action: as its twin COVID-19 pandemic appears to be receding, the obesity and dysmetabolism pandemic continues to rage on. Metabolism. 2022;133:155217.

13. Lee CH, Kang GM, Kim MS. Mechanisms of Weight Control by Primary Cilia. Mol Cells. 2022;45(4):169-76.

14. Han YM, Kang GM, Byun K, Ko HW, Kim J, Shin M-S, et al. Leptin-promoted cilia assembly is critical for normal energy balance. Journal of Clinical Investigation. 2014;124(5):2193-7.

15. Mill P, Christensen ST, Pedersen LB. Primary cilia as dynamic and diverse signalling hubs in development and disease. Nat Rev Genet. 2023;24(7):421-41.

16. Sanchez I, Dynlacht BD. Cilium assembly and disassembly. Nat Cell Biol. 2016;18(7):711-7.

17. Mirvis M, Siemers KA, Nelson WJ, Stearns TP. Primary cilium loss in mammalian cells occurs predominantly by whole-cilium shedding. PLoS Biology. 2019;17(7):e3000381.

18. Macarelli V, Leventea E, Merkle FT. Regulation of the length of neuronal primary cilia and its potential effects on signalling. Trends Cell Biol. 2023.

19. Ávalos Y, Hernández-Cáceres MP, Lagos P, Pinto-Nuñez D, Rivera P, Burgos P, et al. Palmitic acid control of ciliogenesis modulates insulin signaling in hypothalamic neurons through an autophagy-dependent mechanism. Cell Death & Disease. 2022;13(7):659.

20. Kang GM, Han YM, Ko HW, Kim J, Oh BC, Kwon I, Kim M-S. Leptin Elongates Hypothalamic Neuronal Cilia via Transcriptional Regulation and Actin Destabilization*. Journal of Biological Chemistry. 2015;290(29):18146-55.

21. Seo S, Guo D-F, Bugge K, Morgan DA, Rahmouni K, Sheffield VC. Requirement of Bardet-Biedl syndrome proteins for leptin receptor signaling. Human Molecular Genetics. 2009;18(7):1323-31.

22. Puric E, Nilsson UJ, Anderluh M. Galectin-8 inhibition and functions in immune response and tumor biology. Med Res Rev. 2024;44(5):2236-65.

23. Zick Y. Galectin-8, cytokines, and the storm. Biochemical Society Transactions. 2022;50(1):135-49.

24. Perez-Moreno E, Oyanadel C, de la Pena A, Hernandez R, Perez-Molina F, Metz C, et al. Galectins in epithelial-mesenchymal transition: roles and mechanisms contributing to tissue repair, fibrosis and cancer metastasis. Biol Res. 2024;57(1):14.

25. Barake F, Soza A, González A. Galectins in the brain: advances in neuroinflammation, neuroprotection and therapeutic opportunities. Current Opinion in Neurology. 2020;33(3):381-90.

26. Pardo E, Cárcamo C, Martín RU-S, Ciampi E, Segovia-Miranda F, Curkovic-Peña C, et al. Galectin-8 as an immunosuppressor in experimental autoimmune encephalomyelitis and a target of human early prognostic antibodies in multiple sclerosis. PLoS ONE. 2017;12(6):e0177472.

27. Pardo E, Barake F, Godoy JA, Oyanadel C, Espinoza S, Metz C, et al. GALECTIN-8 Is a Neuroprotective Factor in the Brain that Can Be Neutralized by Human Autoantibodies. Molecular Neurobiology. 2019;56(11):7774-88.

28. Ideo H, Matsuzaka T, Nonaka T, Seko A, Yamashita K. Galectin-8-N-domain Recognition Mechanism for Sialylated and Sulfated Glycans*. Journal of Biological Chemistry. 2011;286(13):11346-55.

29. Kumar S, Frank M, Schwartz-Albiez R. Understanding the specificity of human Galectin-8C domain interactions with its glycan ligands based on molecular dynamics simulations. PLoS One. 2013;8(3):e59761.

30. Elola MT, Ferragut F, Cardenas Delgado VM, Nugnes LG, Gentilini L, Laderach D, et al. Expression, localization and function of galectin-8, a tandem-repeat lectin, in human tumors. Histol Histopathol. 2014;29(9):1093-105.

31. Cárcamo C, Pardo E, Oyanadel C, Bravo-Zehnder M, Bull P, Cáceres M, et al. Galectin-8 binds specific beta1 integrins and induces polarized spreading highlighted by asymmetric lamellipodia in Jurkat T cells. Experimental cell research. 2005;312(4):374-86.

32. Oyanadel C, Holmes C, Pardo E, Retamal C, Shaughnessy R, Smith P, et al. Galectin-8 induces partial epithelial–mesenchymal transition with invasive tumorigenic capabilities involving a FAK/EGFR/proteasome pathway in Madin–Darby canine kidney cells. Molecular Biology of the Cell. 2018;29(5):557-74.

33. Chao J-T, Gui P, Zamponi GW, Davis GE, Davis MJ. Spatial association of the Cav1.2 calcium channel with α5β1-integrin. American Journal of Physiology-Cell Physiology. 2011;300(3):C477-C89.

34. Gui P, Wu X, Ling S, Stotz SC, Winkfein RJ, Wilson E, et al. Integrin Receptor Activation Triggers Converging Regulation of Cav1.2 Calcium Channels by c-Src and Protein Kinase A Pathways*. Journal of Biological Chemistry. 2006;281(20):14015-25.

35. Wu X, Davis GE, Meininger GA, Wilson E, Davis MJ. Regulation of the L-type Calcium Channel by α5β1 Integrin Requires Signaling between Focal Adhesion Proteins*. Journal of Biological Chemistry. 2001;276(32):30285-92.

36. Yang Y, Wu X, Gui P, Wu J, Sheng J-Z, Ling S, et al. α5β1 Integrin Engagement Increases Large Conductance, Ca2+-activated K+ Channel Current and Ca2+ Sensitivity through c-src-mediated Channel Phosphorylation*. Journal of Biological Chemistry. 2010;285(1):131-41.

37. Bae E, Huang P, Muller-Greven G, Hambardzumyan D, Sloan AE, Nowacki AS, et al. Integrin alpha3beta1 promotes vessel formation of glioblastoma-associated endothelial cells through calcium-mediated macropinocytosis and lysosomal exocytosis. Nat Commun. 2022;13(1):4268.

38. Pugacheva EN, Jablonski SA, Hartman TR, Henske EP, Golemis EA. HEF1-Dependent Aurora A Activation Induces Disassembly of the Primary Cilium. Cell. 2007;129(7):1351-63.

39. Plotnikova OV, Pugacheva EN, Dunbrack RL, Golemis EA. Rapid calcium-dependent activation of Aurora-A kinase. Nature Communications. 2010;1(1):64.

40. Plotnikova OV, Nikonova AS, Loskutov YV, Kozyulina PY, Pugacheva EN, Golemis EA. Calmodulin activation of Aurora-A kinase (AURKA) is required during ciliary disassembly and in mitosis. Molecular Biology of the Cell. 2012;23(14):2658-70.

41. Bertolin G, Tramier M. Insights into the non-mitotic functions of Aurora kinase A: more than just cell division. Cell Mol Life Sci. 2020;77(6):1031-47.

42. Korobeynikov V, Deneka AY, Golemis EA. Mechanisms for nonmitotic activation of Aurora-A at cilia. Biochem Soc Trans. 2017;45(1):37-49.

43. Hablitz LM, Nedergaard M. The Glymphatic System: A Novel Component of Fundamental Neurobiology. J Neurosci. 2021;41(37):7698-711.

44. Dalvi PS, Nazarians-Armavil A, Tung S, Belsham DD. Immortalized neurons for the study of hypothalamic function. Am J Physiol Regul Integr Comp Physiol. 2011;300(5):R1030-52.

45. Hansen JN, Rassmann S, Stüven B, Jurisch-Yaksi N, Wachten D. CiliaQ: a simple, open-source software for automated quantification of ciliary morphology and fluorescence in 2D, 3D, and 4D images. The European Physical Journal E, Soft Matter. 2021;44(2):18.

46. Raychowdhury MK, McLaughlin M, Ramos AJ, Montalbetti N, Bouley R, Ausiello DA, Cantiello HF. Characterization of Single Channel Currents from Primary Cilia of Renal Epithelial Cells*. Journal of Biological Chemistry. 2005;280(41):34718-22.

47. Marchant V, Droguett A, Valderrama G, Burgos ME, Carpio D, Kerr B, et al. Tubular overexpression of Gremlin in transgenic mice aggravates renal damage in diabetic nephropathy. Am J Physiol Renal Physiol. 2015;309(6):F559-68.

48. De Rosa R, Garcia AA, Braschi C, Capsoni S, Maffei L, Berardi N, Cattaneo A. Intranasal administration of nerve growth factor (NGF) rescues recognition memory deficits in AD11 anti-NGF transgenic mice. Proc Natl Acad Sci U S A. 2005;102(10):3811-6.

49. Wu S, Stogios N, Hahn M, Navagnanavel J, Emami Z, Chintoh A, et al. Outcomes and clinical implications of intranasal insulin on cognition in humans: A systematic review and meta-analysis. PLoS One. 2023;18(6):e0286887.

50. Falcone JA, Salameh TS, Yi X, Cordy BJ, Mortell WG, Kabanov AV, Banks WA. Intranasal Administration as a Route for Drug Delivery to the Brain: Evidence for a Unique Pathway for Albumin. Journal of Pharmacology and Experimental Therapeutics. 2014;351(1):54-60.

51. Morton GJ, Meek TH, Schwartz MW. Neurobiology of food intake in health and disease. Nat Rev Neurosci. 2014;15(6):367-78.

52. Bar S, Grenez C, Nguyen M, de Broca B, Bernard E, Abou-Arab O, et al. Predicting postoperative complications with the respiratory exchange ratio after high-risk noncardiac surgery: A prospective cohort study. Eur J Anaesthesiol. 2020;37(11):1050-7.

53. Kabra DG, Pfuhlmann K, Garcia-Caceres C, Schriever SC, Casquero Garcia V, Kebede AF, et al. Hypothalamic leptin action is mediated by histone deacetylase 5. Nat Commun. 2016;7:10782.

54. Barrow H, Guo X, Wandall HH, Pedersen JW, Fu B, Zhao Q, et al. Serum Galectin-2, -4, and -8 Are Greatly Increased in Colon and Breast Cancer Patients and Promote Cancer Cell Adhesion to Blood Vascular Endothelium. Clinical Cancer Research. 2011;17(22):7035-46.

55. Yu TB, Dodd S, Yu LG, Subramanian S. Serum galectins as potential biomarkers of inflammatory bowel diseases. PLoS One. 2020;15(1):e0227306.

56. Carlsson S, Oberg CT, Carlsson MC, Sundin A, Nilsson UJ, Smith D, et al. Affinity of galectin-8 and its carbohydrate recognition domains for ligands in solution and at the cell surface. Glycobiology. 2007;17(6):663-76.

57. Bershteyn M, Atwood SX, Woo W-M, Li M, Oro AE. MIM and Cortactin Antagonism Regulates Ciliogenesis and Hedgehog Signaling. Developmental Cell. 2010;19(2):270-83.

58. Drummond ML, Li M, Tarapore E, Nguyen TTL, Barouni BJ, Cruz S, et al. Actin polymerization controls cilia-mediated signaling. The Journal of Cell Biology. 2018;217(9):3255-66.

59. Breit A, Besik V, Solinski HJ, Muehlich S, Glas E, Yarwood SJ, Gudermann T. Serine-727 phosphorylation activates hypothalamic STAT-3 independently from tyrosine-705 phosphorylation. Mol Endocrinol. 2015;29(3):445-59.

60. Chen Y, Wang X. miRDB: an online database for prediction of functional microRNA targets. Nucleic Acids Res. 2020;48(D1):D127-D31.

61. Lozano-Bartolomé J, Llauradó G, Portero-Otin M, Altuna-Coy A, Rojo-Martínez G, Vendrell J, et al. Altered Expression of miR-181a-5p and miR-23a-3p Is Associated With Obesity and TNFα-Induced Insulin Resistance. The Journal of Clinical Endocrinology & Metabolism. 2018;103(4):1447-58.

62. Silveira A, Gomes J, Roque F, Fernandes T, de Oliveira EM. MicroRNAs in Obesity-Associated Disorders: The Role of Exercise Training. Obes Facts. 2022;15(2):105-17.

63. Lee YH, Kim YB, Kim KS, Jang M, Song HY, Jung SH, et al. Lateral hypothalamic leptin receptor neurons drive hunger-gated food-seeking and consummatory behaviours in male mice. Nat Commun. 2023;14(1):1486.

64. Bernard A, Ojeda Naharros I, Yue X, Mifsud F, Blake A, Bourgain-Guglielmetti F, et al. MRAP2 regulates energy homeostasis by promoting primary cilia localization of MC4R. JCI Insight. 2023;8(2).

65. Jeong SH, Jang JH, Lee YB. Drug delivery to the brain via the nasal route of administration: exploration of key targets and major consideration factors. J Pharm Investig. 2023;53(1):119-52.

66. Benedict C, Kern W, Schultes B, Born J, Hallschmid M. Differential sensitivity of men and women to anorexigenic and memory-improving effects of intranasal insulin. J Clin Endocrinol Metab. 2008;93(4):1339-44.

67. Derkach KV, Ivantsov AO, Chistyakova OV, Sukhov IB, Buzanakov DM, Kulikova AA, Shpakov AO. Intranasal Insulin Restores Metabolic Parameters and Insulin Sensitivity in Rats with Metabolic Syndrome. Bull Exp Biol Med. 2017;163(2):184-9.

68. Walia V, Cuenca A, Vetter M, Insinna C, Perera S, Lu Q, et al. Akt Regulates a Rab11-Effector Switch Required for Ciliogenesis. Developmental Cell. 2019;50(2):229-46.e7.

69. Romaniuk MA, Tribulatti MV, Cattaneo V, Lapponi MJ, Molinas FC, Campetella O, Schattner M. Human platelets express and are activated by galectin-8. The Biochemical journal. 2010;432(3):535-47.

70. Ran J, Yang Y, Li D, Liu M, Zhou J. Deacetylation of alpha-tubulin and cortactin is required for HDAC6 to trigger ciliary disassembly. Sci Rep. 2015;5:12917.

71. Kwon O, Kim KW, Kim MS. Leptin signalling pathways in hypothalamic neurons. Cell Mol Life Sci. 2016;73(7):1457-77.

72. Massardo L, Metz C, Pardo E, Mezzano V, Babul M, Jarpa E, et al. Autoantibodies against galectin-8: their specificity, association with lymphopenia in systemic lupus erythematosus and detection in rheumatoid arthritis and acute inflammation. Lupus. 2009;18(6):539-46.

73. Vicuna L, Pardo E, Curkovic C, Doger R, Oyanadel C, Metz C, et al. Galectin-8 binds to LFA-1, blocks its interaction with ICAM-1 and is counteracted by anti-Gal-8 autoantibodies isolated from lupus patients. Biol Res. 2013;46(3):275-80.

74. Norambuena A, Metz C, Vicuña L, Silva A, Pardo E, Oyanadel C, et al. Galectin-8 Induces Apoptosis in Jurkat T Cells by Phosphatidic Acid-mediated ERK1/2 Activation Supported by Protein Kinase A Down-regulation*. Journal of Biological Chemistry. 2009;284(19):12670-9.

75. Flemming A. How the brain regulates inflammation. Nat Rev Immunol. 2024;24(6):378.

76. Dennis JW, Nabi IR, Demetriou M. Metabolism, cell surface organization, and disease. Cell. 2009;139(7):1229-41.

77. Cerliani JP, Blidner AG, Toscano MA, Croci DO, Rabinovich GA. Translating the 'Sugar Code' into Immune and Vascular Signaling Programs. Trends Biochem Sci. 2017;42(4):255-73.

78. Andre S, Kaltner H, Manning JC, Murphy PV, Gabius HJ. Lectins: getting familiar with translators of the sugar code. Molecules. 2015;20(2):1788-823.

79. Hesketh GG, Dennis JW. N-acetylglucosamine: more than a silent partner in insulin resistance. Glycobiology. 2017;27(7):595-8.

80. Pedersen HK, Gudmundsdottir V, Nielsen HB, Hyotylainen T, Nielsen T, Jensen BA, et al. Human gut microbes impact host serum metabolome and insulin sensitivity. Nature. 2016;535(7612):376-81.

81. Allendorf DH, Brown GC. Neu1 Is Released From Activated Microglia, Stimulating Microglial Phagocytosis and Sensitizing Neurons to Glutamate. Front Cell Neurosci. 2022;16:917884.

82. Nomura K, Vilalta A, Allendorf DH, Hornik TC, Brown GC. Activated Microglia Desialylate and Phagocytose Cells via Neuraminidase, Galectin-3, and Mer Tyrosine Kinase. J Immunol. 2017;198(12):4792-801.

83. Hong MH, Lin WH, Weng IC, Hung YH, Chen HL, Chen HY, et al. Intracellular galectins control cellular responses commensurate with cell surface carbohydrate composition. Glycobiology. 2019;30(1):49-57.

84. Hong MH, Weng IC, Li FY, Lin WH, Liu FT. Intracellular galectins sense cytosolically exposed glycans as danger and mediate cellular responses. J Biomed Sci. 2021;28(1):16.

85. Fradin D, Boëlle P-Y, Belot M-P, Lachaux F, Tost J, Besse C, et al. Genome-Wide Methylation Analysis Identifies Specific Epigenetic Marks In Severely Obese Children. Scientific Reports. 2017;7(1):46311.

86. Ollikainen M, Ismail K, Gervin K, Kyllönen A, Hakkarainen A, Lundbom J, et al. Genome-wide blood DNA methylation alterations at regulatory elements and heterochromatic regions in monozygotic twins discordant for obesity and liver fat. Clinical Epigenetics. 2015;7(1):39.

87. Fougerat A, Pan X, Smutova V, Heveker N, Cairo CW, Issad T, et al. Neuraminidase 1 activates insulin receptor and reverses insulin resistance in obese mice. Molecular Metabolism. 2018;12:76-88.

88. Mori D, Yamada M, Mimori-Kiyosue Y, Shirai Y, Suzuki A, Ohno S, et al. An essential role of the aPKC-Aurora A-NDEL1 pathway in neurite elongation by modulation of microtubule dynamics. Nat Cell Biol. 2009;11(9):1057-68.

89. Arslanhan MD, Rauniyar N, Yates JR, 3rd, Firat-Karalar EN. Aurora Kinase A proximity map reveals centriolar satellites as regulators of its ciliary function. EMBO Rep. 2021;22(8):e51902.

90. Tian Z, Miyata K, Tabata M, Yano M, Tazume H, Aoi J, et al. Nifedipine increases energy expenditure by increasing PGC-1α expression in skeletal muscle. Hypertension Research. 2011;34(11):1221-7.

91. Zhang H, Wang X, Wan Y, Liu L, Zhou J, Li P, Xu B. Discovery of N-Arylsulfonyl-Indole-2-Carboxamide Derivatives as Galectin-3 and Galectin-8 C-Terminal Domain Inhibitors. ACS Med Chem Lett. 2023;14(9):1257-65.

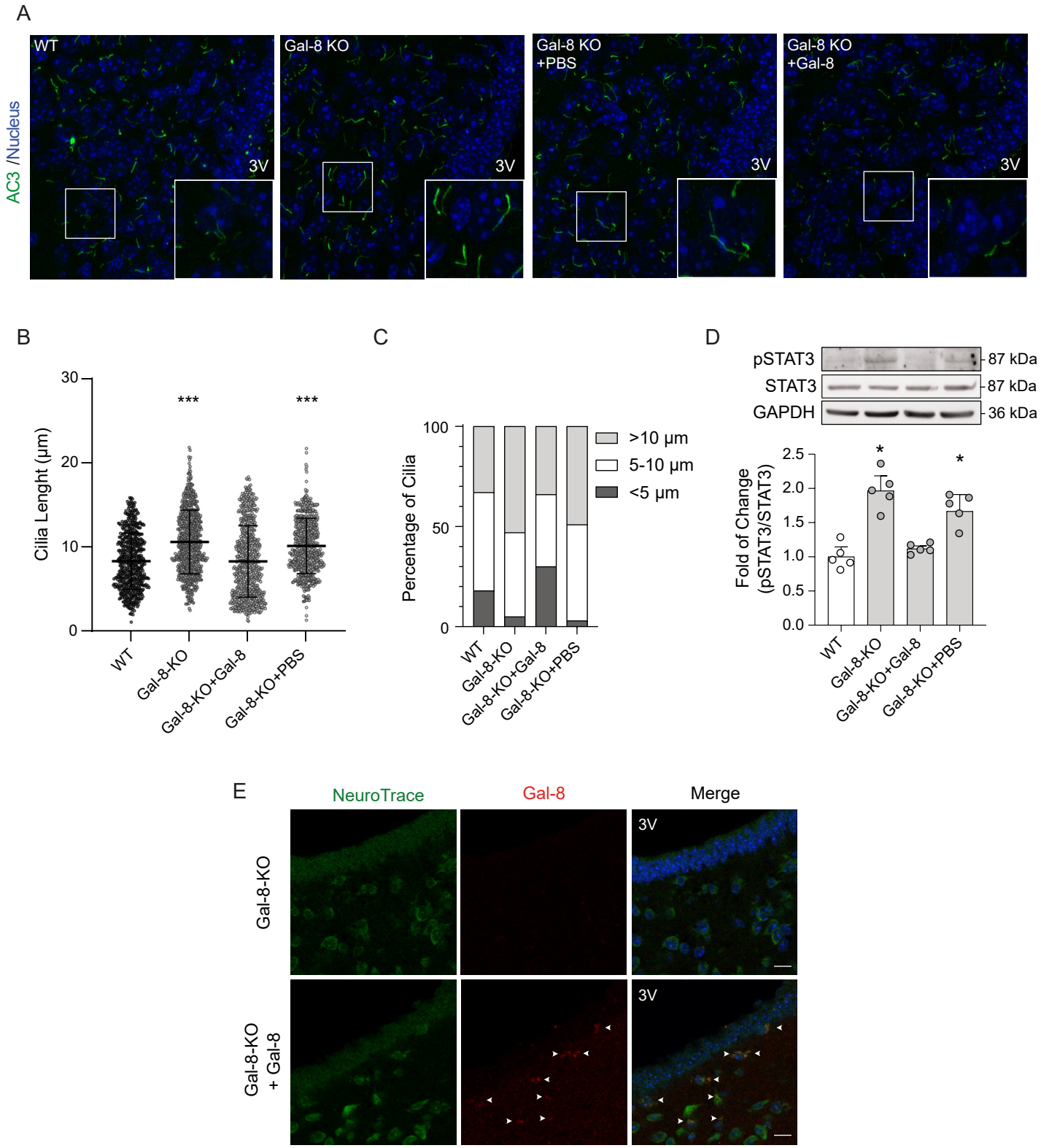
A
AC3 /Nucleus
WT
Gal-8 KO
Gal-8 KO +PBS
Gal-8 KO +Gal-8
3V
B
Cilia Lenght (µm)
***
WT
Gal-8-KO
Gal-8-KO+Gal-8
Gal-8-KO+PBS
C
Percentage of Cilia
>10 µm
5-10 µm
<5 µm
D
pSTAT3
STAT3
GAPDH
87 kDa
36 kDa
Fold of Change (pSTAT3/STAT3)
*
E
NeuroTrace
Gal-8
Merge
Gal-8-KO
Gal-8-KO + Gal-8

Figure 1

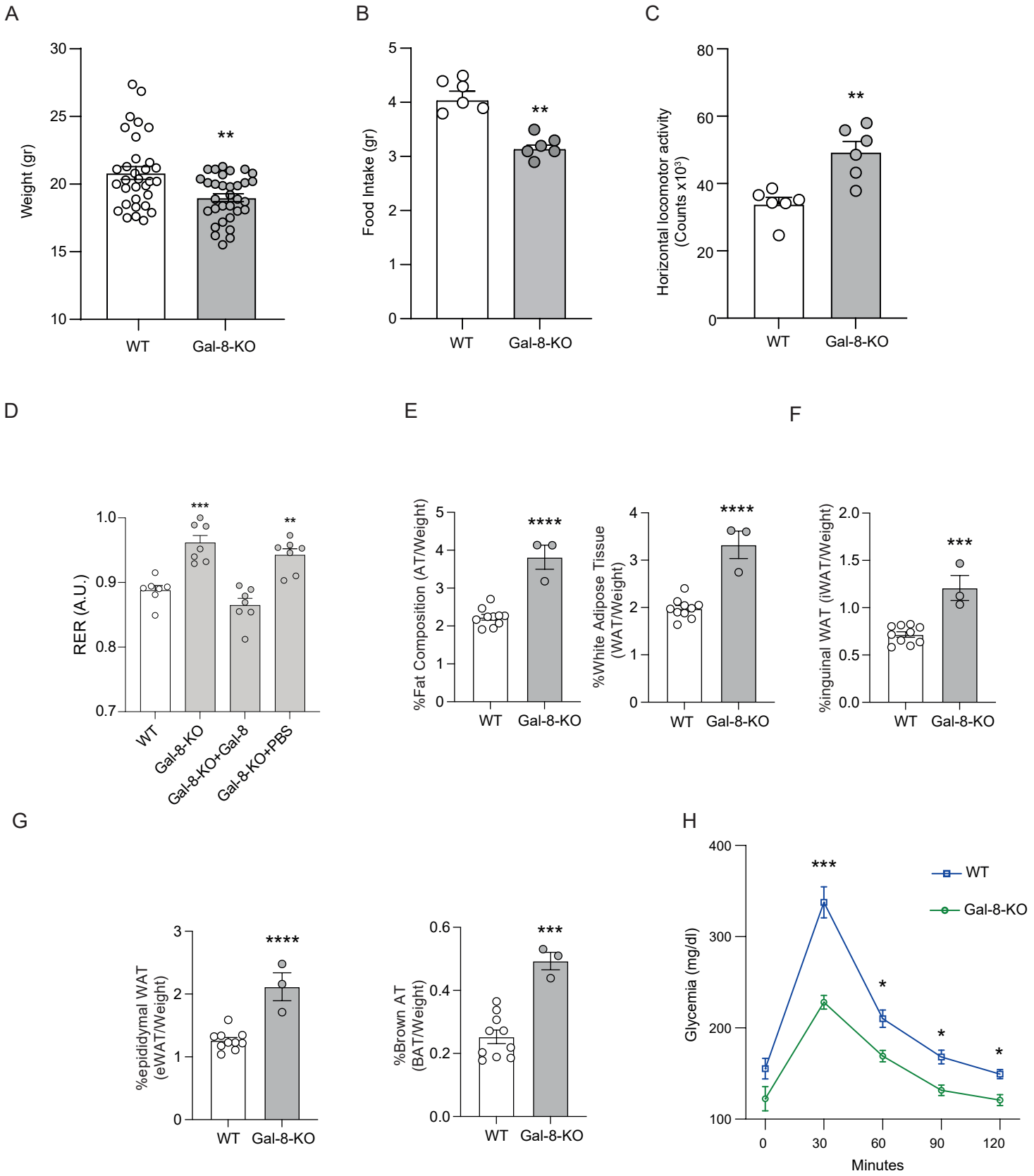
A
Weight (gr)
30
25
20
15
10
**
WT
Gal-8-KO
B
Food Intake (gr)
5
4
3
2
1
0
**
WT
Gal-8-KO
C
Horizontal locomotor activity (Counts x10³)
80
60
40
20
0
**
WT
Gal-8-KO
D
RER (A.U.)
1.0
0.9
0.8
0.7
***
**
WT
Gal-8-KO
Gal-8-KO+Gal-8
Gal-8-KO+PBS
E
%Fat Composition (AT/Weight)
5
4
3
2
1
0
****
WT
Gal-8-KO
%White Adipose Tissue (WAT/Weight)
4
3
2
1
0
****
WT
Gal-8-KO
F
%inguinal WAT (iWAT/Weight)
2.0
1.5
1.0
0.5
0.0
***
WT
Gal-8-KO
G
%epididymal WAT (eWAT/Weight)
3
2
1
0
****
WT
Gal-8-KO
%Brown AT (BAT/Weight)
0.6
0.4
0.2
0.0
***
WT
Gal-8-KO
H
Glycemia (mg/dl)
400
300
200
100
***
*
*
*
WT
Gal-8-KO
0
30
60
90
120
Minutes

Figure 2

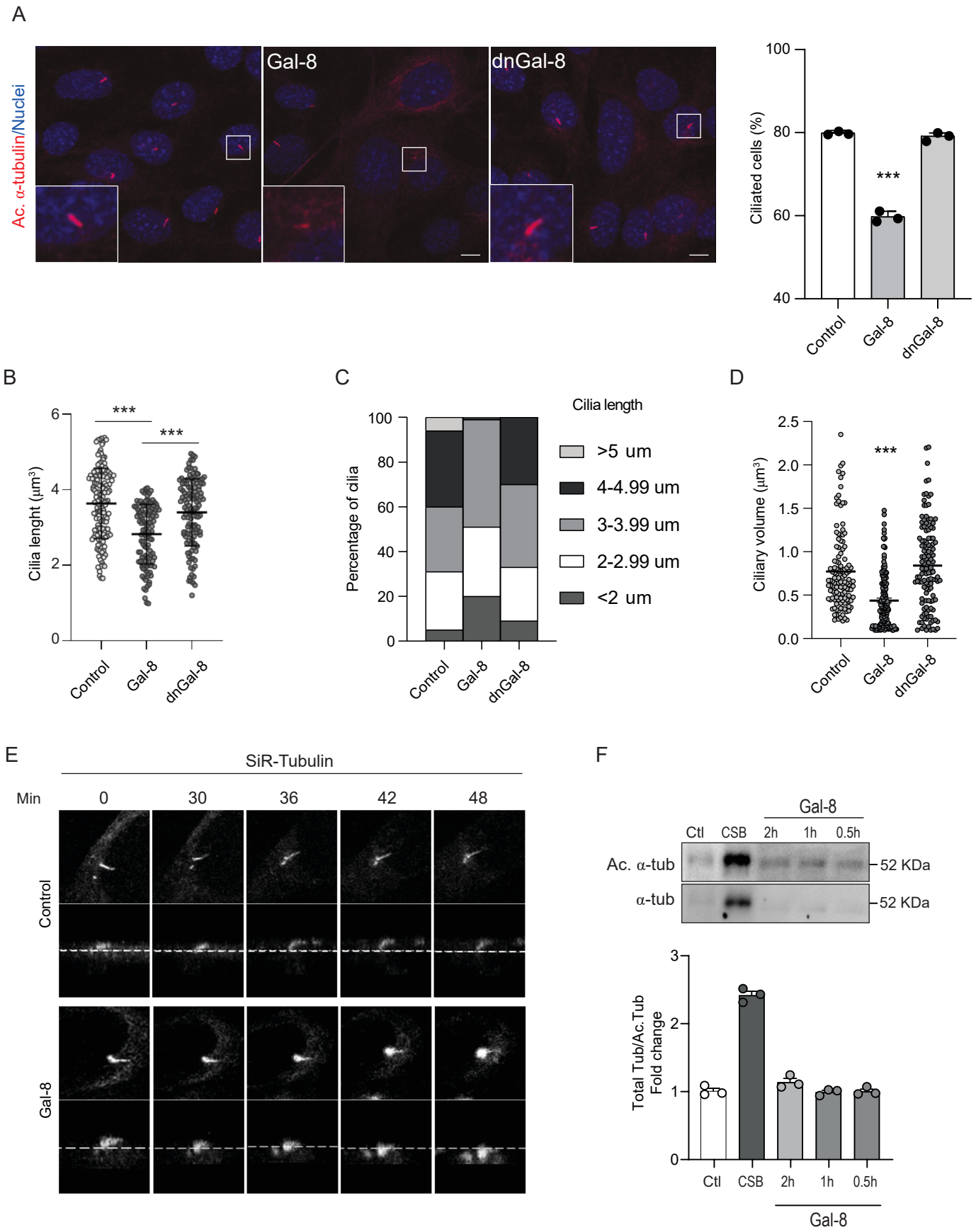
A
Ac. α-tubulin/Nuclei
Gal-8
dnGal-8
Ciliated cells (%)
100
80
60
40
***
Control
Gal-8
dnGal-8
B
Cilia lenght (µm³)
6
4
2
0
***
***
Control
Gal-8
dnGal-8
C
Percentage of cilia
100
80
60
40
20
0
Cilia length
>5 um
4-4.99 um
3-3.99 um
2-2.99 um
<2 um
Control
Gal-8
dnGal-8
D
Ciliary volume (µm³)
2.5
2.0
1.5
1.0
0.5
0.0
***
Control
Gal-8
dnGal-8
E
SiR-Tubulin
Min
0
30
36
42
48
Control
Gal-8
F
Gal-8
Ctl
CSB
2h
1h
0.5h
Ac. α-tub
α-tub
52 KDa
52 KDa
Total Tub/Ac.Tub
Fold change
3
2
1
0
Ctl
CSB
2h
1h
0.5h
Gal-8

Figure 3

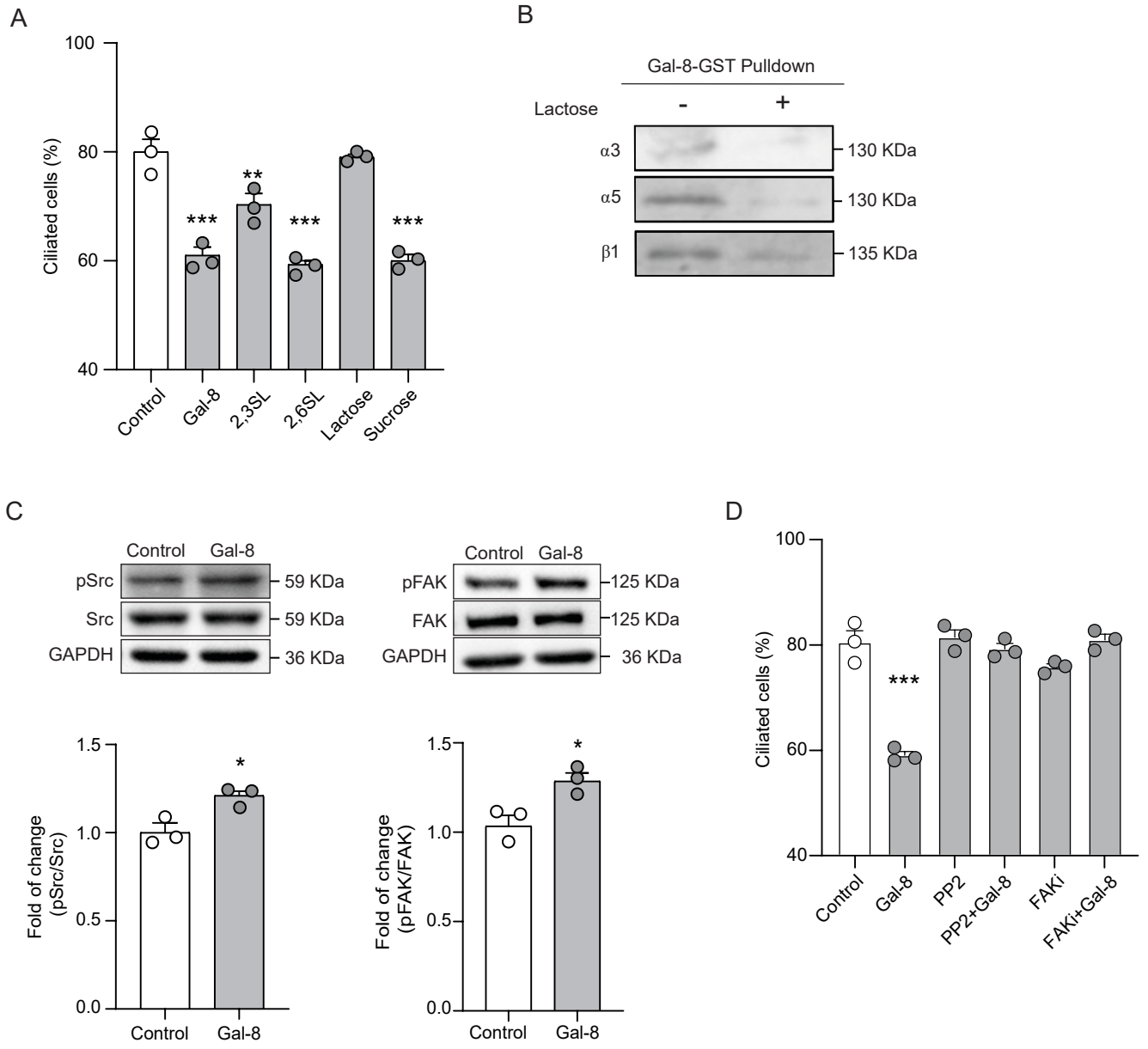
A
Ciliated cells (%)
100
80
60
40
***
**
***
***
Control
Gal-8
2,3SL
2,6SL
Lactose
Sucrose
B
Gal-8-GST Pulldown
Lactose
-
+
α3
α5
β1
130 KDa
130 KDa
135 KDa
C
Control
Gal-8
pSrc
Src
GAPDH
59 KDa
59 KDa
36 KDa
pFAK
FAK
GAPDH
125 KDa
125 KDa
36 KDa
Fold of change (pSrc/Src)
Fold of change (pFAK/FAK)
1.5
1.0
0.5
0.0
*
*
D
Ciliated cells (%)
***
Control
Gal-8
PP2
PP2+Gal-8
FAKi
FAKi+Gal-8

Figure 4

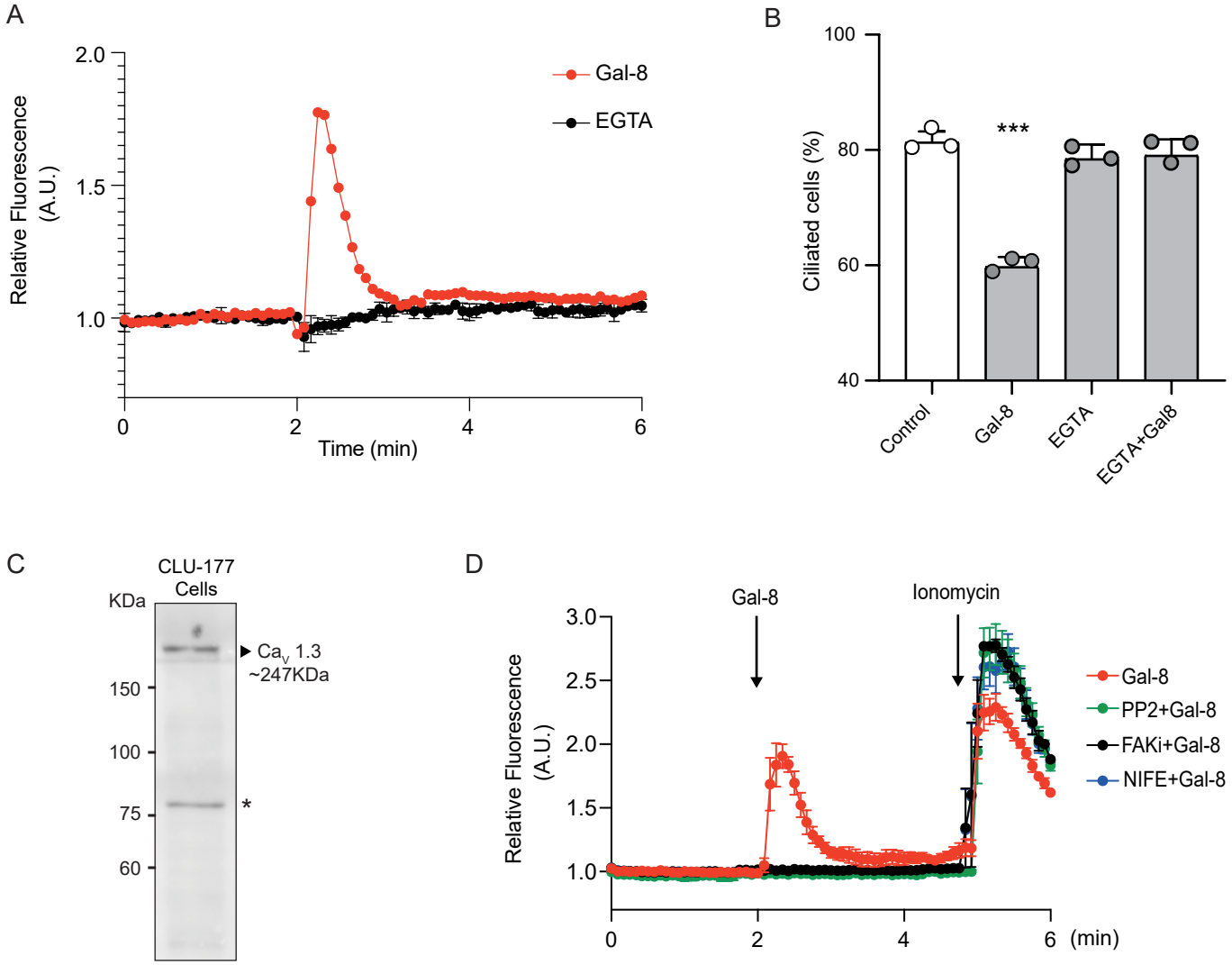
A
Relative Fluorescence (A.U.)
2.0
1.5
1.0
Gal-8
EGTA
0
2
4
6
Time (min)
B
Ciliated cells (%)
100
80
60
40
***
Control
Gal-8
EGTA
EGTA+Gal8
C
CLU-177 Cells
KDa
150
100
75
60
Cav 1.3
~247KDa
*
D
Relative Fluorescence (A.U.)
3.0
2.5
2.0
1.5
1.0
Gal-8
Ionomycin
Gal-8
PP2+Gal-8
FAKi+Gal-8
NIFE+Gal-8
0
2
4
6
(min)

Figure 5

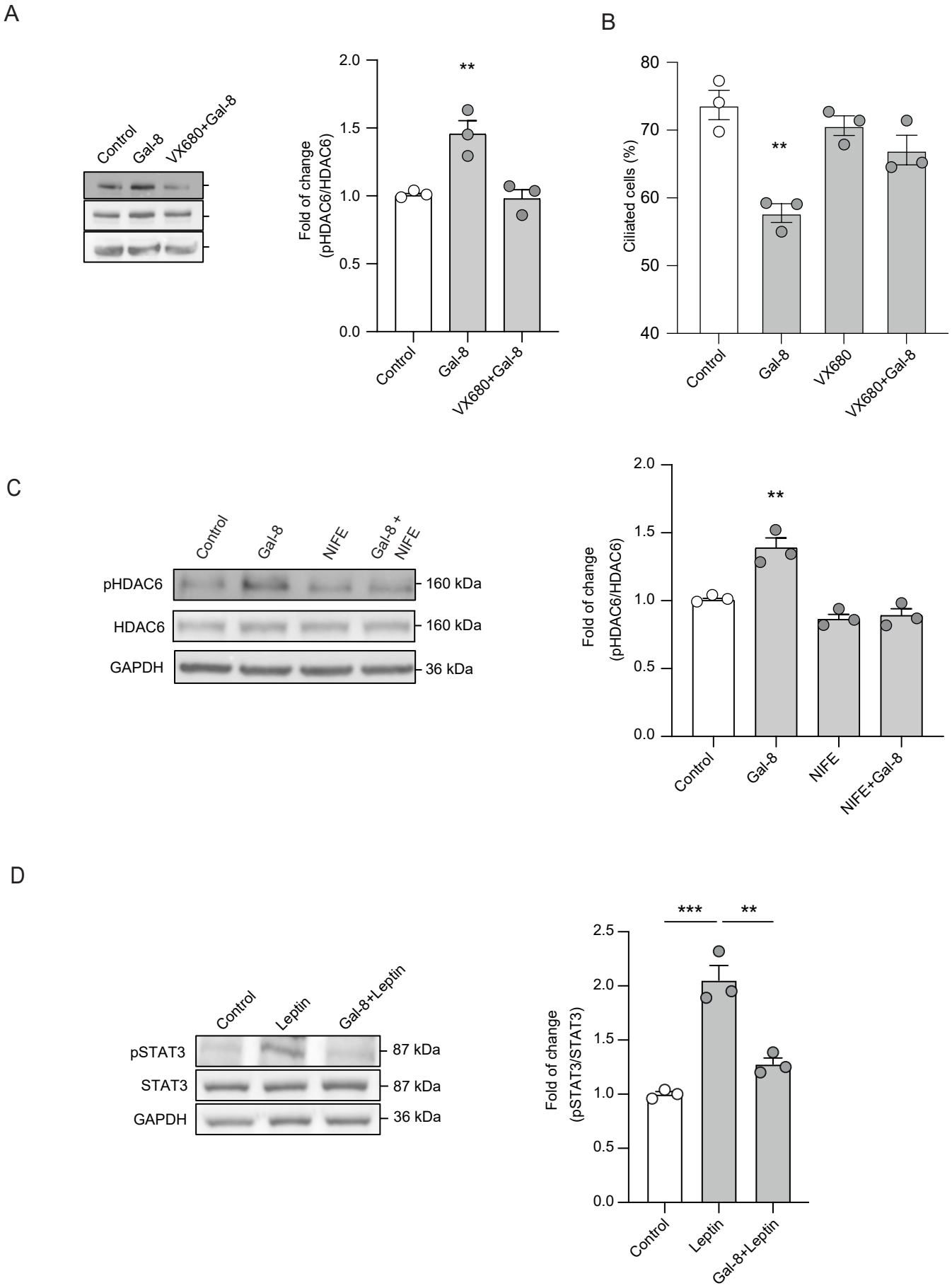
A
Control
Gal-8
VX680+Gal-8
Fold of change
(pHDAC6/HDAC6)
2.0
1.5
1.0
0.5
0.0
**
Control
Gal-8
VX680+Gal-8
B
Ciliated cells (%)
80
70
60
50
40
**
Control
Gal-8
VX680
VX680+Gal-8
C
Control
Gal-8
NIFE
Gal-8 +
NIFE
pHDAC6
HDAC6
GAPDH
160 kDa
160 kDa
36 kDa
Fold of change
(pHDAC6/HDAC6)
2.0
1.5
1.0
0.5
0.0
**
Control
Gal-8
NIFE
NIFE+Gal-8
D
Control
Leptin
Gal-8+Leptin
pSTAT3
STAT3
GAPDH
87 kDa
87 kDa
36 kDa
Fold of change
(pSTAT3/STAT3)
2.5
2.0
1.5
1.0
0.5
0.0
***
**
Control
Leptin
Gal-8+Leptin

Figure 6